frontiers in Chemistry

ORIGINAL RESEARCH
published: 04 December 2019
doi: 10.3389/fchem.2019.00766

Nitrogen-Doped Ketjenblack Carbon Supported Co_3O_4 Nanoparticles as a Synergistic Electrocatalyst for Oxygen Reduction Reaction

Gao Cheng[1†], Guanliang Liu[1†], Peng Liu[1†], Liya Chen[1], Shengbo Han[1], Jiaxi Han[1], Fei Ye[1], Wei Song[1], Bang Lan[2], Ming Sun[1] and Lin Yu[1]*

[1] Key Laboratory of Clean Chemistry Technology of Guangdong Regular Higher Education Institutions, School of Chemical Engineering and Light Industry, Guangdong University of Technology, Guangzhou, China, [2] School of Chemistry and Environment, Jiaying University, Meizhou, China

Developing a highly active and cost-effective cathode electrocatalyst with strong stability for oxygen reduction reaction (ORR) is extremely necessary. In this work, we reported a facile synthetic path to prepare a hybrid nanostructure formed of nitrogen-doped Ketjenblack carbon (N-KC) supported Co_3O_4 nanoparticles (Co_3O_4/N-KC), which could be used as a promising and stable electrocatalyst for ORR. Compared with the physical mixture of Co_3O_4 and N-KC and pure N-KC samples, the resulting Co_3O_4/N-KC nanohybrid afforded remarkably superb ORR activity with a half-wave potential of 0.82 V (vs. reversible hydrogen electrode, RHE) and a limiting current density of 5.70 mA cm^{-2} in KOH solution (0.1 M). Surprisingly, the Co_3O_4/N-KC sample possessed a similar electrocatalytic activity but better durability to the 20 wt% Pt/C catalyst. The remarkable ORR activity of the Co_3O_4/N-KC nanohybrid was mainly due to the strong coupling effect between Co_3O_4 and N-KC, the N species dopant, high electroconductivity, and the large BET surface area. Our work enlightens the exploitation of advanced Co_3O_4/carbon hybrid material alternative to the Pt-based electrocatalysts.

Keywords: Co_3O_4, ketjenblack carbon, nitrogen dopant, electronic coupling effect, electrocatalyst, oxygen reduction reaction, zinc-air batteries

OPEN ACCESS

Edited by:
Zexing Wu,
Qingdao University of Science and Technology, China

Reviewed by:
Youwen Liu,
Huazhong University of Science and Technology, China
Likai Wang,
Shandong University of Technology, China

****Correspondence:***
Lin Yu
gych@gdut.edu.cn

† These authors have contributed equally to this work

Specialty section:
This article was submitted to Catalysis and Photocatalysis, a section of the journal Frontiers in Chemistry

Received: *01 October 2019*
Accepted: *24 October 2019*
Published: *04 December 2019*

Citation:
Cheng G, Liu G, Liu P, Chen L, Han S, Han J, Ye F, Song W, Lan B, Sun M and Yu L (2019) Nitrogen-Doped Ketjenblack Carbon Supported Co_3O_4 Nanoparticles as a Synergistic Electrocatalyst for Oxygen Reduction Reaction. Front. Chem. 7:766. doi: 10.3389/fchem.2019.00766

INTRODUCTION

With an ever-growing demand in electricity energy supply, electrical energy storage (EES) technology has witnessed booming progress by rapidly exploitative next-generation electrochemical power storage devices, such as supercapacitors (Zhong et al., 2015; Wang S. et al., 2019), Li-ion batteries (Liu et al., 2017; Xia et al., 2017), Zn-ion batteries (Yu et al., 2019), and metal-air batteries (Cheng and Chen, 2012). More recently, zinc-air batteries (ZABs), which generate electricity via the direct redox chemical reaction between Zn and O_2, have been considered a promising and advanced energy storage device owing to its non-toxicity, low price, reliable safety, as well as a large theoretical energy density of 1,218 Wh kg^{-1} (Fu et al., 2018d; Zhu et al., 2018). Currently, the efficient energy conversion of ZABs is still dramatically hindered by the slow oxygen reduction reaction (ORR) kinetics at cathode, which significantly restricts the quality of ZABs (Guo et al., 2018). To lower the energy barrier of ORR, the rational design and preparation of highly efficient electrocatalysts, is inevitably desirable. Traditionally, the Pt-group metals are the benchmark

catalysts for O_2 electrocatalysis, but their practical utility is greatly plagued by a limited natural shortage, prohibitive prices, and unsatisfying durability (Li et al., 2016; Wang et al., 2017b; Song et al., 2018; Vargas-Ordaz et al., 2019). This issue has led scientists to explore suitable and cost-efficient ORR catalysts with high-efficiency electrochemical activity and stability.

In recent years, lots of inexpensive alternatives have been reported to possess decent ORR activities, including non-precious metals and their alloys (Lee et al., 2018), carbon-based materials (Wu et al., 2016a; Fu et al., 2018b), Fe-N-C (Sun et al., 2018; Wang C. et al., 2019), and transition metal oxides and their derivatives (Meng et al., 2014; Tian et al., 2015; Miura et al., 2016; Jin et al., 2019), etc. Particularly, Co_3O_4 has gained growing interest with merits of plentiful resources, eco-friendliness, and mix-valence (Co^{2+} and Co^{3+}) (Xiao et al., 2013). However, because of its inherent poor conductivity, the ORR activities of Co_3O_4 catalysts are still not satisfactory and underperform the Pt/C catalyst (Yu et al., 2017). Moreover, the Co_3O_4 electrocatalysts usually suffer from agglomeration and dissolution during the long-term cycle, giving rise to the insufficient ORR stability (Han et al., 2018). To circumvent these obstacles, carbon-based materials (e.g., graphene, Ketjenblack, and g-C_3N_4) with excellent conductivity and corrosion resistance were usually employed as supporters in depositing the nanostructured Co_3O_4, which markedly boosts ORR activity and stability (Liang et al., 2011; Liu K. et al., 2016; Li et al., 2017; Wang et al., 2018). Compared to other carbon-based materials, Ketjenblack (KB) has become very attractive by virtue of its favorable physic-chemical properties (e.g., outstanding conductivity, high surface area, and good structural stability), making it an excellent carrier for supporting the Co_3O_4 nanocrystallines. For example, the Co_3O_4/N-doped KB nanocomposite was successfully obtained through a hydrothermal approach followed by a thermal decomposition process, which achieved a positive half-wave potential [0.79 V vs. reversible hydrogen electrode (RHE)] with surprisingly stability (Liu K. et al., 2016). The Co_3O_4/Co-N modified KB nanohybrid was fabricated through a direct pyrolysis method, and displayed a half-wave potential of ∼0.80 V vs. RHE with strong durability (Li et al., 2017). Overall, the synthesis of the above reported hybrid ORR catalysts required a long reaction time and complicated procedures, and these catalysts still exhibited dissatisfactory ORR activities. Thereby, the development of a simple strategy for the synthesis of a Co_3O_4/KC hybrid electrocatalyst under facile conditions, as well as significantly improved ORR performance, is highly challenging and valuable.

In this context, our facile synthetic strategy realized a hybrid nanostructure of Co_3O_4 nanoparticles anchored on a N-doped KC (N-KC) substrate, on which a promising and stable electrocatalytic activity for ORR was accomplished. Due to the strong coupling effect between Co_3O_4 and N-KC, the N species dopant, high electroconductivity and large BET surface area, the resultant Co_3O_4/N-KC nanohybrid exhibited evidently superior ORR catalytic performance than the Co_3O_4 + N-KC and pure N-KC control samples in an alkaline condition. More importantly, such a hybrid Co_3O_4/N-KC electrocatalyst showed a comparable ORR performance (half-wave potential and diffusion-limiting current) to that of Pt/C. Additionally, the Co_3O_4/N-KC nanohybrid manifested better long-term stability than the Pt/C after 12 h of chronoamperometric measurement. The successful fabrication of the Co_3O_4/N-KC hybrid material presented a guideline for the preparation of an effective Pt-free ORR cathode catalyst.

EXPERIMENTAL DETAILS

Preparation of N-KC

First, 1.0 g of KC (Ketjenblack, Japan LION, EC-600JD) was slowly added into the concentrated HNO_3 (50 mL) solution and then heated at 70°C for 6 h. After being cooled to room temperature, KC was washed with deionized water to remove residual surface HNO_3, and dried at 60°C overnight. Second, 1 g of as-prepared KC and 0.5 g of melamine were well-mixed, sintered at 700°C for 2 h in a N_2 atmosphere, and cooled naturally, thus the N-KC was finally formed.

Preparation of Co_3O_4/N-KC Nanocomposite and Pure Co_3O_4 Nanocubes

Typically, 20.0 mg of $Co(CH_3COO)_2{\cdot}4H_2O$ was dissolved in 35 ml distilled water to form a clear $Co(CH_3COO)_2$ solution, and then N-KC (70.0 mg) was added into the $Co(CH_3COO)_2$ solution. The obtained slurry was further stirred for at least 20 min. The mixed suspension was rapidly transferred to a Teflon-lined autoclave (50 ml). After hydrothermally reacting at 120°C for 12 h, the resultant precipitate was centrifuged with deionized water and alcohol, and subsequently dried in an oven to yield the Co_3O_4/N-KC nanostructure.

Pure Co_3O_4 nanocubes were prepared via the same procedures as making a Co_3O_4/N-KC sample without adding any N-KC.

Characterization

The phase purity and crystallinity of products were characterized by X-ray powder diffraction (XRD, Bruker D8 advance) from $2\theta = 10–80°$ (Cu Kα radiation). The shape, microstructure and surface composition of the resulting samples were analyzed by field-emission scanning electron microscopy (FE-SEM, Hitach, SU8220), field-emission transmission electron microscopy (FE-TEM, FEI Talos F200S) and X-ray photoelectron spectroscopy (XPS, Escalab 250Xi). The surface area of Co_3O_4/K-NC was calculated from N_2 adsorption-desorption isotherms at −196°C, attained using an ASAP 2020 surface area analyzer (Micromeritics, USA). The metal contents in the Co_3O_4/K-NC were measured on an inductively coupled plasma-optical emission spectrometer (ICP-OES, Agilent 725). The conductivity of the Co_3O_4/K-NC and Pt/C samples was measured using a typical two electrode system (ZAHNER, Germany).

Electrocatalytic Tests

The electrochemical measurements were performed using a rotating device (GAMRY RDE710) with a three-electrode system, lined with a computer-controlled electrochemical workstation (CHI 760E). The working electrode was a glassy carbon

(GC) electrode (5.6 mm in diameter) with the catalyst coating. Typically, 7 mg of the sample was dispersed in the mixed solvent (1.0 ml) containing 950 μl of ethanol and 50 μl of Nafion (5 wt%, DuPont), which was then ultrasonicated for ∼60 min. The as-obtained ink (7.0 μl) was loaded on the wording electrode and dried in an oven (60°C) for testing, which afforded a mass loading of ∼0.20 mg cm^{-2}. A platinum foil (1 × 1 cm^2) and Ag/AgCl electrode were used as the counter electrode and reference electrode, respectively. Before each measurement, a high-purity N_2/O_2 flow was used to saturate the aqueous solution (0.1 M KOH) for at least 30 min. The electrocatalytic performances of the samples were tested using a cyclic voltammogram (CV), linear sweep voltammogram (LSV), and a chronoamperometry method. All the obtained potentials were transformed to the RHE scale according to the following Nernst equation (Equation 1).

$$E_{RHE} = E_{Ag/AgCl} + 0.059pH + E^{o}_{Ag/AgCl} \quad (1)$$

The electron transfer number (n) and the percentage of peroxide species (HO_2^-%) were calculated, separately, through the Equation 2 and Equation 3 as follows:

$$n = 4\frac{I_d}{I_d + \frac{I_r}{N}} \quad (2)$$

$$HO_2^-\% = 200\ \frac{\frac{I_r}{N}}{I_d + \frac{I_r}{N}} \quad (3)$$

where I_d, I_r, and N represent the disk current, the ring current and the collection efficiency of the RRDE, respectively.

RESULTS AND DISCUSSION

Structure and Composition Characterization

Our synthetic approach of the Co_3O_4/N-KC nanocomposite is illustrated in **Figure 1A**. This method involved two main steps: (i) the synthesis of nitrogen doped KC via calcining the KC with melamine at 700°C under N_2 flow; and (ii) the growth of Co_3O_4 nanoparticles on the N-KC surface through the hydrothermal approach. The crystal structures of N-KC and Co_3O_4/N-KC were ascertained by the XRD, as shown in **Figure 1B**. Obviously, a strong and broad diffraction peak located at ∼24.8° can be seen in the XRD patterns of N-KC and Co_3O_4/N-KC, which is characteristic of highly graphitic carbon (Ge et al., 2019). For Co_3O_4/N-KC, the diffraction peaks at 18.9°, 31.1°, 36.8°, 44.6°, 55.5°, 59.2°, and 65.0° correspond well to the (111), (220), (311), (400), (422), (511), and (440) planes of the spinel Co_3O_4 phase (JCPDS: 742120). In the crystalline framework of Co_3O_4 (**Figure 1C**), Co^{2+} cations and Co^{3+} cations occupy the tetrahedral interstices and octahedral interstices, respectively, both of which are coordinated by O^{2-} anions (Xie et al., 2009). Moreover, based on the Scherrer's equation, the particle size of Co_3O_4 nanocrystallines on N-KC surface is calculated to be ∼26.2 nm.

FESEM and FETEM were used to analyze the microstructure of the prepared Co_3O_4/N-KC. As observed from the FESEM images (**Figure 2A** and **Figure S1**), we can speculate that the Co_3O_4 nanocrystallines are well-dispersed throughout the N-KC framework (Liu K. et al., 2016). The high-angle annular dark-field scanning TEM (HAADF-STEM) clearly indicates the presence of Co_3O_4 nanoparticles on the N-KC surface (**Figure 2B**). Moreover, the FETEM image (**Figure 2C**) further reveals that the Co_3O_4 nanocrystallines are densely immobilized on the N-KC surface, exhibiting an average size of ∼28.7 nm in the range of 10–50 nm (inset of **Figure 2C**), which well-approaches the value computed by the XRD result. Shown in **Figure 2D** is a high magnification of the Co_3O_4 nanoparticles from a section of **Figure 2C**. The corresponding HR-FETEM image (inset of **Figure 2D**) corroborates that the interlayer spacing is 2.43 Å, which corresponds to the (311) plane of Co_3O_4. Such a hybrid nanostructure of Co_3O_4/N-KC was characterized via the N_2 adsorption-desorption measurement. On the basis of the Brunauer-Emmett-Teller (BET) approach, the Co_3O_4/N-KC nanohybrid presents an extremely large BET surface area of 813.69 $m^2\ g^{-1}$, as calculated from **Figure S2**.

The in-depth information on the surface chemical compositions of Co_3O_4/N-KC was further studied by the XPS technique. The full survey spectrum in **Figure 3A** confirms the presence of four kinds of elements (Co, O, N, and C) that can be detected in the Co_3O_4/N-KC sample. The existence of N 1s peak demonstrates that the N atoms were successfully doped into the carbon skeleton. In the high-resolution Co 2p spectrum (**Figure 3B**), two peaks at 780.6 and 795.7 eV are attributed to the Co $2p_{3/2}$ and Co $2p_{1/2}$ core levels. In particular, the Co $2p_{3/2}$ can be broken down into three components of Co^{3+} (780.3 eV), Co^{2+} (782.5 eV), and satellite (785.4 and 789.1 eV), respectively (Ren et al., 2018). **Figure 3C** presents the O 1s XPS spectrum of Co_3O_4/N-KC, which is decomposed into three different types of surface oxygen species including lattice oxygen (O_α = 530.2 eV), adsorbed oxygen (O_β = 532.3 eV), and chemisorbed water (O_γ = 533.8 eV) (Liu K. et al., 2016). As displayed in **Figure 3D**, the deconvolution of C 1s spectrum exhibits three peaks at 284.7, 285.4, and 288.8 eV, which can be attributable to C=C, C=N, and C-N of the carbon skeleton, respectively (Han et al., 2018). Similarly, the high-resolution spectrum of N 1s can also be fitted to three various forms (**Figure 3E**), belonging to the pyridinic N (398.5 eV), pyridinic N (399.9 eV), and graphitic N (400.8 eV), respectively (Xie et al., 2015). The Co 2p results of Co_3O_4/N-KC were compared to that of a pure Co_3O_4 sample, and the detailed structural and morphological results of the Co_3O_4 sample are also given in **Figure S3**. As shown in **Figure 3F**, it should be noted that the higher binding energy shift of Co $2p_{3/2}$ and Co $2p_{1/2}$ peaks can clearly be seen for the Co_3O_4/N-KC. This result suggests that there was a strong electronic coupling between Co_3O_4 and N-KC, induced by the heterogeneous interface between the Co_3O_4 nanoparticles and the N-KC framework (Wu et al., 2016b; Fu et al., 2018c). Taking the above results (XRD, FETEM and XPS) into account, the Co_3O_4 nanoparticles immobilized on the N-KC skeleton were successfully prepared through our facile synthetic route.

ORR Activity and Stability Tests

The electrochemical catalytic performances of the Co_3O_4/N-KC nanocomposite for ORR was conducted in KOH medium (0.1 M). The cyclic voltammogram (CV) of Co_3O_4/N-KC was

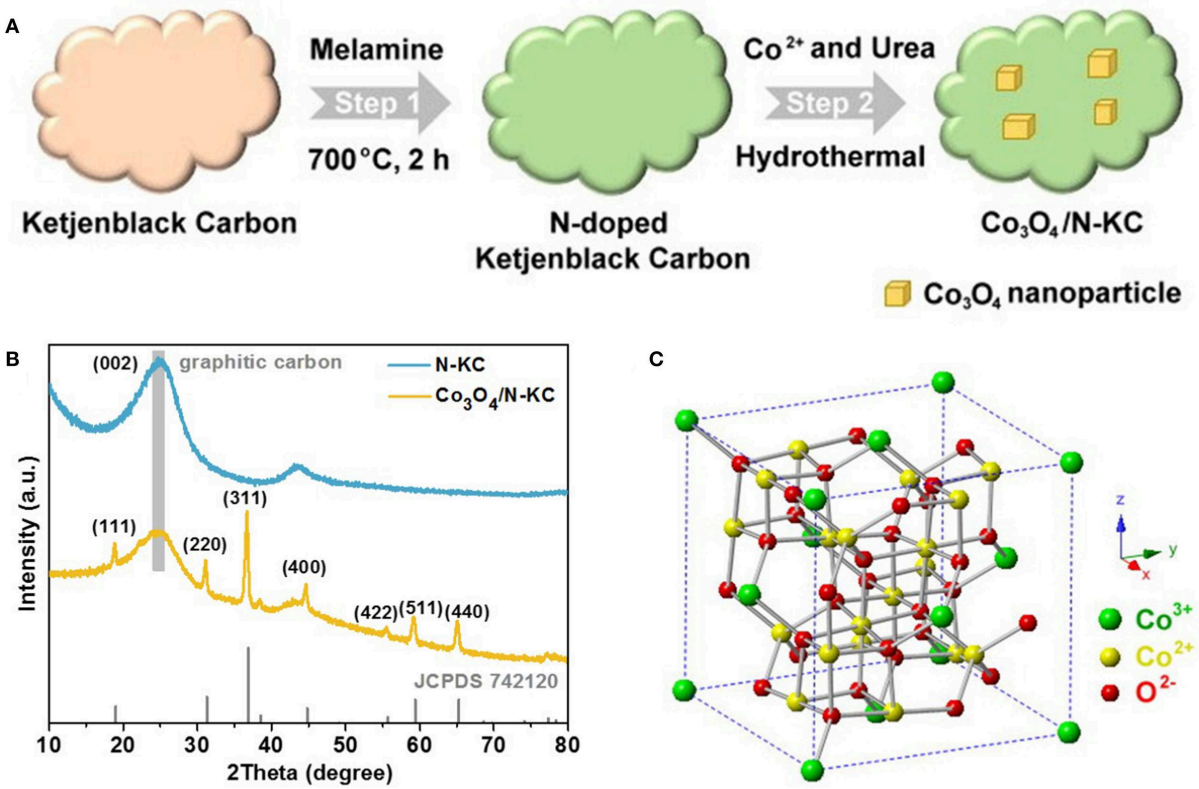

FIGURE 1 | (A) Schematic illustration of the synthesis procedures of Co_3O_4/N-KC; **(B)** XRD patterns of N-KC and Co_3O_4/N-KC; **(C)** Crystalline framework of Co_3O_4.

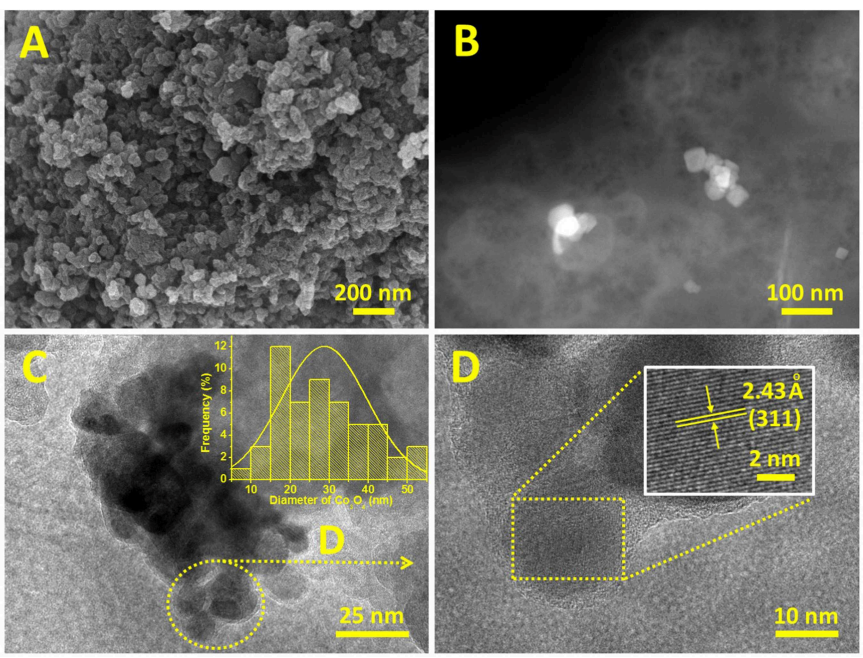

FIGURE 2 | (A) FESEM and **(B)** HAADF-STEM images of Co_3O_4/N-KC; **(C)** FETEM and size distribution (inset) of Co_3O_4 nanoparticles; **(D)** FETEM and HR-FETEM (inset) images of Co_3O_4 nanoparticles.

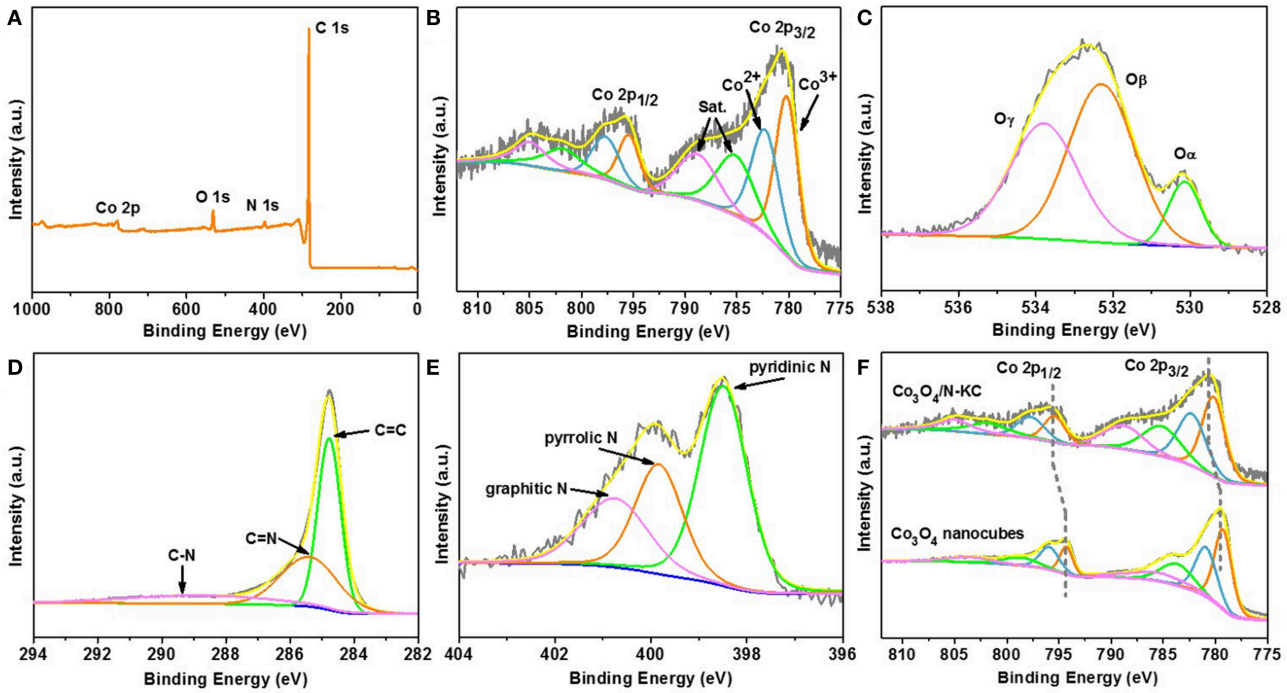

FIGURE 3 | (A) XPS full survey spectrum of Co_3O_4/N-KC; High-resolution XPS spectra of Co_3O_4/N-KC at **(B)** Co 2p, **(C)** O 1s, **(D)** C 1s, and **(E)** N 1s; **(F)** XPS spectra of Co 2p in Co_3O_4/N-KC and pure Co_3O_4.

first carried out and compared with other control samples, including a physical mixture of Co_3O_4 nanocubes and N-KC (Co_3O_4 + N-KC) and pure N-KC. As depicted in **Figure 4A**, the CV curves in N_2-saturated electrolyte on all the samples show no redox peaks. However, in the O_2-saturated electrolyte, the corresponding CV curves display distinct cathodic peaks, belonging to the ORR electrocatalysis. In particular, the ORR peak of Co_3O_4/N-KC is located at 0.78 V, which is the most positive among the three samples, suggesting its extraordinary electrocatalytic activity. The ORR performances of the Co_3O_4/N-KC, Co_3O_4 + N-KC, and N-KC were further investigated by LSV using a rotating ring-disk electrode (RRDE) at 1,600 rpm. Moreover, the LSV measurement of commercial Pt/C was also evaluated. **Figure 4B** displays the LSV curves measured by the ring and disk. Based on the data collected from the disk, the Co_3O_4/N-KC presents a high onset potential (E_{onset}) and half-wave potential (E_{half}) of 0.87 and 0.82 V, respectively, which are much more positive than those of Co_3O_4 + N-KC (E_{onset} = 0.84 and E_{half} = 0.77 V) and N-KC (E_{onset} = 0.81 and E_{half} = 0.73 V). In addition, the limiting current density at 0.3 V follows the trend of Co_3O_4/N-KC (5.70 mA cm^{-2}) > Co_3O_4 + N-KC (5.51 mA cm^{-2}) > N-KC (5.36 mA cm^{-2}). Though the E_{onset} of Co_3O_4/N-KC is lower than that of Pt/C (0.91 V), the values of E_{half} and limiting current density afforded by Co_3O_4/N-KC are well-close to those of Pt/C (0.83 V and 5.72 mA cm^{-2}). Remarkably, the ring current density of Co_3O_4/N-KC also highly approaches that of Pt/C, which is obviously lower than those of Co_3O_4 + N-KC and N-KC. The results above collectively testify that the prepared Co_3O_4/N-KC nanohybrid delivers a remarkable electrocatalytic activity for ORR in alkaline media, which rivals those of the excellent non-noble metal electrocatalysts reported previously (**Table S1**).

To deeply understand the ORR reaction kinetics for the Co_3O_4/N-KC nanohybrid, LSV tests at different rotating speeds (400–2,500 rpm) were further conducted, as illustrated in **Figure S4**. As expected, the current density value increases with the enhancement of rotation speed since the diffusion distance becomes shortened at an improved rotation rate (Soren et al., 2019). **Figure 4C** displays the K-L lines of Co_3O_4/N-KC based on the rotation-speed-dependent currents under various potentials (0.3–0.7 V), and all of them possess excellent linearity. Significantly, these lines exhibit nearly similar slopes to the green line, implying that Co_3O_4/N-KC favors a quasi-four-electron ($4e^-$) ORR mechanism (Wu et al., 2018). **Figure 4D** presents the electron transfer number (n) and percentage of peroxide species (HO_2^-%) calculated from the ring and disk currents. Within the potential range from 0.40 to 0.75 V, the calculated n of Co_3O_4/N-KC is ~3.82, which is almost the same with the Pt/C (~3.87), again revealing that the ORR catalyzed by Co_3O_4/N-KC was mainly through a quasi-$4e^-$ pathway. Furthermore, the determined HO_2^-% of Co_3O_4/N-KC (~8.35%) is substantially lower than that of Co_3O_4 + N-KC (~17.03%) and N-KC (~36.32%), showing high electrocatalytic efficiency for the ORR.

The ascendant ORR electrocatalytic activity of Co_3O_4/N-KC can be further demonstrated by the Tafel slope (**Figure 5A**). Amongst all the samples, the Co_3O_4/N-KC displays the smallest

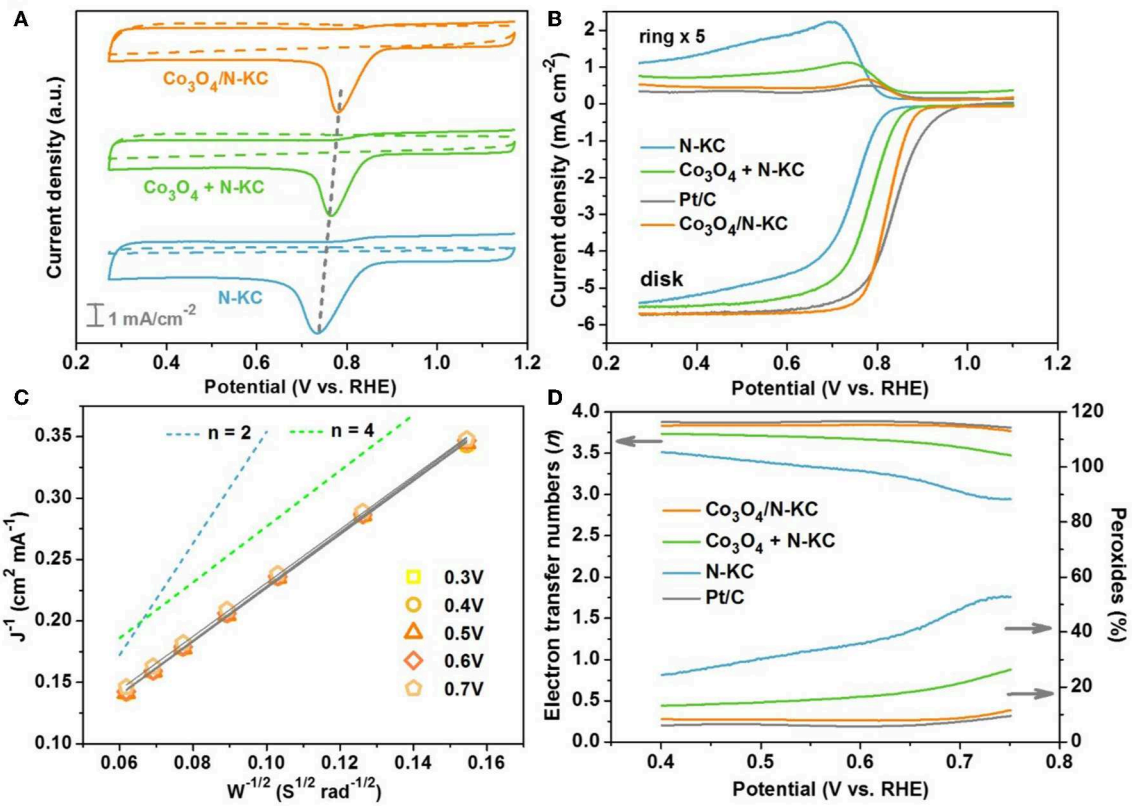

FIGURE 4 | (A) CV curves of Co_3O_4/N-KC, Co_3O_4 + N-KC and N-KC samples in both N_2-saturated and O_2-saturated KOH solution (0.1 M); **(B)** LSV curves of Co_3O_4/N-KC, Co_3O_4 + N-KC, N-KC, and Pt/C at 1,600 rpm; **(C)** K-L plots of Co_3O_4/N-KC at various potentials; **(D)** Electron transfer number and percentage of peroxides for Co_3O_4/N-KC.

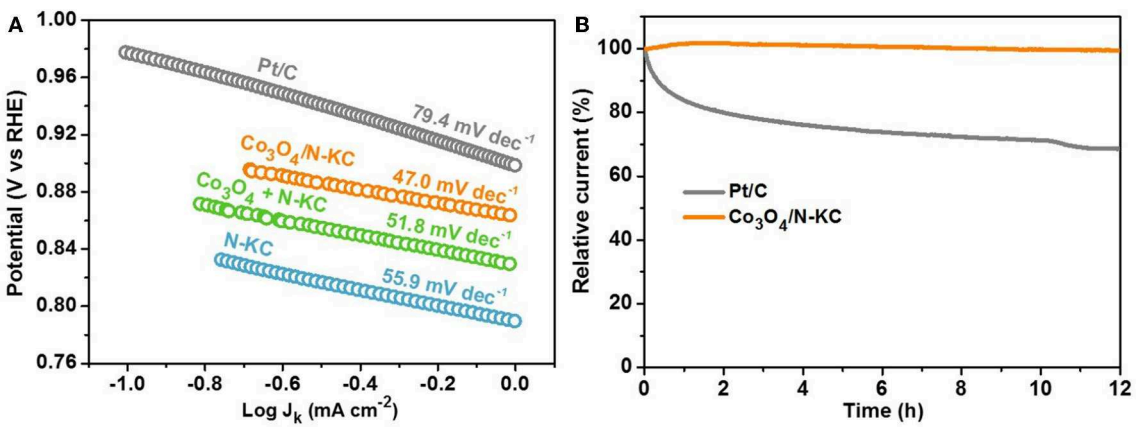

FIGURE 5 | (A) Tafel plots of the four samples; **(B)** Chronoamperometry (12 h) of the Co_3O_4/N-KC and Pt/C samples maintained at a constant potential of 0.5 V in O_2-saturated KOH (0.1 M).

slope (47.0 mV dec^{-1}), which is indicative of its favorable ORR dynamic rate (Liu J. et al., 2016; Wang et al., 2016). Beyond that, chronoamperometry was measured to compare the ORR durability of the Co_3O_4/N-KC and Pt/C catalysts (**Figure 5B**). After testing for a continuous period of 12 h, the Co_3O_4/N-KC undergoes a negligible current decrease of 0.51%, while a distinct current fading (31.38%) is achieved for Pt/C. The superb ORR activity as well as outstanding durability of Co_3O_4/N-KC signify that the Co_3O_4/N-KC nanohybrid can be applied as a promising cathode catalyst in ZABs.

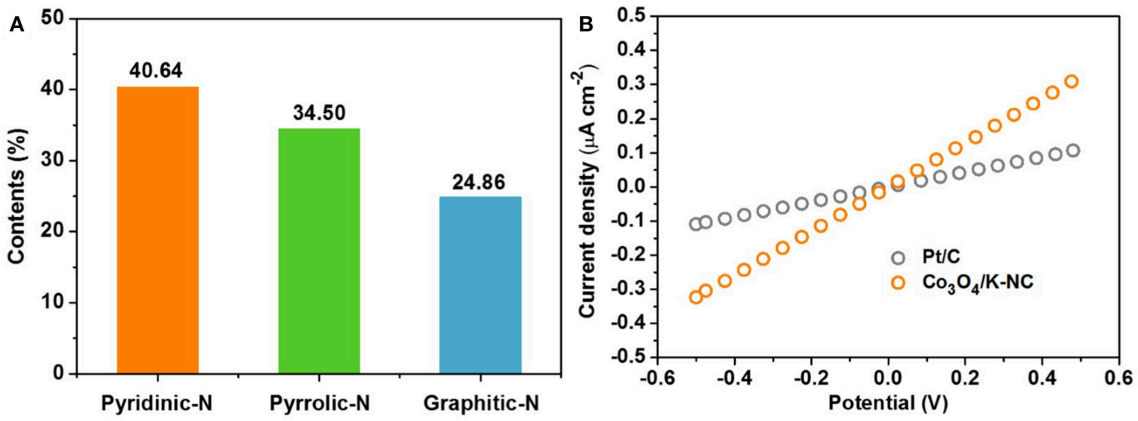

FIGURE 6 | (A) The contents of different kinds of N species in Co_3O_4/N-KC sample; **(B)** Comparison of I–V curves of the Co_3O_4/N-KC and Pt/C samples.

Origin of ORR Activity of Co_3O_4/N-KC

Considering the corresponding physico-chemical characterizations for the Co_3O_4/N-KC nanohybrid, its impressive ORR activity could be well-ascribed to the following main aspects: (1) Strong electronic coupling effect. The XPS result, as evidenced through Co 2p spectrum (**Figure 3F**), suggests that a strong electronic coupling exists in the Co_3O_4/N-KC nanohybrid. This strong coupling effect not only guarantees the improved electron transport ability, but also offers highly active electrochemically sites, thereby leading to our hybrid Co_3O_4/N-KC catalyst being more active (Liang et al., 2012). (2) Abundant pyridinic and graphitic N species. The contents of pyridinic, pyrrolic and graphitic N species within the Co_3O_4/N-KC nanohybrid are estimated to be 40.64, 34.50, and 24.86%, respectively (**Figure 6A**). It was demonstrated that both the pyridinic and graphitic N dopants in the carbon skeleton could improve the O_2 capture ability, which further boosted the ORR electrocatalytic process (Xie et al., 2015; Fu et al., 2018a). (3) A highly electroconductive and large BET surface area. The I-V curves of the Co_3O_4/N-KC and Pt/C samples measured by two electrode systems are given in **Figure 6B**. Note that the electrical conductivity of the Co_3O_4/N-KC is even higher than the Pt/C, which may be caused by the direct combination of the Co_3O_4 nanoparticles and the highly conductive N-KC skeleton. Also, the large BET surface area can offer more sufficient contact between catalyst and molecules/ions. Benefiting from these two distinct advantages, the efficient electrochemical reactions of the Co_3O_4/N-KC for ORR can occur (He et al., 2017; Wang et al., 2017a).

CONCLUSION

Altogether, a hybrid nanostructure, Co_3O_4 nanoparticles supported on a K-NC skeleton, was successfully fabricated through a facile strategy for the application of electrocatalytic oxygen reduction. The strong coupling effect, N species dopant, high electroconductivity, and large BET surface area enabled our Co_3O_4/N-KC nanohybrid to be highly efficient, as the ORR cathode electrocatalyst. In contrast to the Co_3O_4 + N-KC and pure N-KC samples, the resultant Co_3O_4/N-KC nanohybrid exhibited splendid ORR electrocatalytic activity in KOH medium, achieving more positive potential values (E_{onset} = 0.87 V and E_{half} = 0.82 V) and larger limited current density (5.70 mA cm^{-2}). What's more, the Co_3O_4/N-KC sample displayed comparable electrocatalytic activity and better stability compared to the Pt/C catalyst.

DATA AVAILABILITY STATEMENT

The datasets generated for this study are available on request from the corresponding author.

AUTHOR CONTRIBUTIONS

GC, GL, PL, and LY designed the project. GC, GL, PL, LC, WS, and BL performed the synthesis and characterization experiments, and data analysis. GL, PL, LC, SH, JH, and FY did the ORR tests and data analysis. MS helped design the ORR tests. GC wrote this manuscript. All authors contributed to editing and discussion of the manuscript.

FUNDING

This work was supported by the National Natural Science Foundation of China (21576054, 21603039); Science and Technology Planning Project of Guangdong Province (2016A010104017); and the Foundation of Higher Education of Guangdong Province (2015KTSCX027, 2018KZDXM031).

SUPPLEMENTARY MATERIAL

The Supplementary Material for this article can be found online at: https://www.frontiersin.org/articles/10.3389/fchem.2019.00766/full#supplementary-material

REFERENCES

Cheng, F., and Chen, J. (2012). Metal-air batteries: from oxygen reduction electrochemistry to cathode catalysts. *Chem. Soc. Rev.* 41, 2172–2192. doi: 10.1039/c1cs15228a

Fu, G., Liu, Y., Chen, Y., Tang, Y., Goodenough, J. B., and Lee, J. M. (2018a). Robust N-doped carbon aerogels strongly coupled with iron-cobalt particles as efficient bifunctional catalysts for rechargeable Zn-air batteries. *Nanoscale* 10, 19937–19944. doi: 10.1039/c8nr05812a

Fu, G., Tang, Y., and Lee, J.-M. (2018b). Recent advances in carbon-based bifunctional oxygen electrocatalysts for Zn-air batteries. *ChemElectroChem* 5, 1424–1434. doi: 10.1002/celc.201800373

Fu, G., Wang, J., Chen, Y., Liu, Y., Tang, Y., Goodenough, J. B., et al. (2018c). Exploring indium-based ternary thiospinel as conceivable high-potential air-cathode for rechargeable Zn-air batteries. *Adv. Energy Mater.* 8:1802263. doi: 10.1002/aenm.201802263

Fu, G., Yan, X., Chen, Y., Xu, L., Sun, D., Lee, J. M., et al. (2018d). Boosting bifunctional oxygen electrocatalysis with 3D graphene aerogel-supported Ni/MnO particles. *Adv. Mater.* 30:1704609. doi: 10.1002/adma.201704609

Ge, L., Wang, D., Yang, P., Xu, H., Xiao, L., Zhang, G. X., et al. (2019). Graphite N-C-P dominated three-dimensional nitrogen and phosphorus co-doped holey graphene foams as high-efficiency electrocatalysts for Zn-air batteries. *Nanoscale* 11, 17010–17017. doi: 10.1039/c9nr04696h

Guo, J., Chen, B., Hao, Q., Nie, J., and Ma, G. (2018). Pod-like structured Co/CoO_x nitrogen-doped carbon fibers as efficient oxygen reduction reaction electrocatalysts for Zn-air battery. *Appl. Surf. Sci.* 456, 959–966. doi: 10.1016/j.apsusc.2018.05.210

Han, X., He, G., He, Y., Zhang, J., Zheng, X., Li, L., et al. (2018). Engineering catalytic active sites on cobalt oxide surface for enhanced oxygen electrocatalysis. *Adv. Energy Mater.* 8:1702222. doi: 10.1002/aenm.201702222

He, J., Wang, M., Wang, W., Miao, R., Zhong, W., Chen, S. Y., et al. (2017). Hierarchical mesoporous NiO/MnO_2@PANI core-shell microspheres, highly efficient and stable bifunctional electrocatalysts for oxygen evolution and reduction reactions. *ACS Appl. Mater. Interf.* 9, 42676–42687. doi: 10.1021/acsami.7b07383

Jin, W., Chen, J., Wu, Z., and Maduraiveeran, G. (2019). Encapsulated spinel $Cu_XCo_{3-X}O_4$ in carbon nanotubes as efficient and stable oxygen electrocatalysts. *Int. J. Hydrogen Energy* 44, 11421–11430. doi: 10.1016/j.ijhydene.2019.03.093

Lee, D. U., Park, M. G., Cano, Z. P., Ahn, W., and Chen, Z. (2018). Hierarchical core-shell nickel cobaltite chestnut-like structures as bifunctional electrocatalyst for rechargeable metal-air batteries. *ChemSusChem* 11, 406–414. doi: 10.1002/cssc.201701832

Li, J., Zhou, Z., Liu, K., Li, F., Peng, Z., Tang, Y., et al. (2017). Co_3O_4/Co-N-C modified ketjenblack carbon as an advanced electrocatalyst for Al-air batteries. *J. Power Sources* 343, 30–38. doi: 10.1016/j.jpowsour.2017.01.018

Li, M., Zhao, Z., Cheng, T., Fortunelli, A., Chen, C.-Y., Yu, R., et al. (2016). Ultrafine jagged platinum nanowires enable ultrahigh mass activity for the oxygen reduction reaction. *Science* 354, 1414–1419. doi: 10.1126/science.aaf9050

Liang, Y., Li, Y., Wang, H., Zhou, J., Wang, J., Regier, T., et al. (2011). Co_3O_4 nanocrystals on graphene as a synergistic catalyst for oxygen reduction reaction. *Nat. Mater.* 10, 780–786. doi: 10.1038/nmat3087

Liang, Y., Wang, H., Zhou, J., Li, Y., Wang, J., Regier, T., et al. (2012). Covalent hybrid of spinel manganese-cobalt oxide and graphene as advanced oxygen reduction electrocatalysts. *J. Am. Chem. Soc.* 134, 3517–3523. doi: 10.1021/ja210924t

Liu, J., Jiang, L., Zhang, T., Jin, J., Yuan, L., and Sun, G. (2016). Activating Mn_3O_4 by morphology tailoring for oxygen reduction reaction. *Electrochim. Acta* 205, 38–44. doi: 10.1016/j.electacta.2016.04.103

Liu, K., Zhou, Z., Wang, H., Huang, X., Xu, J., Tang, Y., et al. (2016). N-doped carbon supported Co_3O_4 nanoparticles as an advanced electrocatalyst for the oxygen reduction reaction in Al-air batteries. *RSC Adv.* 6, 55552–55559. doi: 10.1039/c6ra10486j

Liu, Y., Zhou, T., Zheng, Y., He, Z., Xiao, C., Pang, W. K., et al. (2017). Local electric field facilitates high-performance Li-ion batteries. *ACS Nano* 11, 8519–8526. doi: 10.1021/acsnano.7b04617

Meng, Y., Song, W., Huang, H., Ren, Z., Chen, S. Y., and Suib, S. L. (2014). Structure-property relationship of bifunctional MnO_2 nanostructures: highly efficient, ultra-stable electrochemical water oxidation and oxygen reduction reaction catalysts identified in alkaline media. *J. Am. Chem. Soc.* 136, 11452–11464. doi: 10.1021/ja505186m

Miura, A., Rosero-Navarro, C., Masubuchi, Y., Higuchi, M., Kikkawa, S., and Tadanaga, K. (2016). Nitrogen-rich manganese oxynitrides with enhanced catalytic activity in the oxygen reduction reaction. *Angew. Chem. Int. Ed.* 55, 7963–7967. doi: 10.1002/anie.201601568

Ren, Q., Mo, S., Peng, R., Feng, Z., Zhang, M., Chen, L., et al. (2018). Controllable synthesis of 3D hierarchical Co_3O_4 nanocatalysts with various morphologies for the catalytic oxidation of toluene. *J. Mater. Chem. A* 6, 498–509. doi: 10.1039/C7TA09149D

Song, X., Luo, S., Fan, X., Tang, M., Zhao, X., Chen, W., et al. (2018). Controlled synthesis of PtNi hexapods for enhanced oxygen reduction reaction. *Front. Chem.* 6:468. doi: 10.3389/fchem.2018.00468

Soren, S., Hota, I., Debnath, A. K., Aswal, D. K., Varadwaj, K. S. K., and Parhi, P. (2019). Oxygen reduction reaction activity of microwave mediated solvothermal synthesized CeO_2/g-C_3N_4 nanocomposite. *Front. Chem.* 7:403. doi: 10.3389/fchem.2019.00403

Sun, M., Davenport, D., Liu, H., Qu, J., Elimelech, M., and Li, J. (2018). Highly efficient and sustainable non-precious-metal Fe-N-C electrocatalysts for the oxygen reduction reaction. *J. Mater. Chem. A* 6, 2527–2539. doi: 10.1039/c7ta09187g

Tian, X., Luo, J., Nan, H., Fu, Z., Zeng, J., and Liao, S. (2015). Binary transition metal nitrides with enhanced activity and durability for the oxygen reduction reaction. *J. Mater. Chem. A* 3, 16801–16809. doi: 10.1039/C5TA04410C

Vargas-Ordaz, M., Velázquez-Hernández, I., Bañuelos, J. A., Ledesma-García, J., Álvarez-Contreras, L., Arjona, N., et al. (2019). Synthesis of PtAg bimetallic material as a multi-fuel tolerant electrocatalyst and spectroelectrochemical analysis of its capability to perform the oxygen reduction. *Mater. Today. Energy* 14:100335. doi: 10.1016/j.mtener.2019.07.006

Wang, C., Li, Z., Wang, L., Niu, X., and Wang, S. (2019). Facile synthesis of 3D Fe/N codoped mesoporous graphene as efficient bifunctional oxygen electrocatalysts for rechargeable Zn-air batteries. *ACS Sustain Chem. Eng.* 7, 13873–13885. doi: 10.1021/acssuschemeng.9b02052

Wang, J., Hao, J., Liu, D., Qin, S., Portehault, D., Li, Y., et al. (2017a). Porous boron carbon nitride nanosheets as efficient metal-free catalysts for the oxygen reduction reaction in both alkaline and acidic solutions. *ACS Energy Lett.* 2, 306–312. doi: 10.1021/acsenergylett.6b00602

Wang, L., Tang, Z., Yan, W., Wang, Q., Yang, H., and Chen, S. (2017b). Co@Pt core@shell nanoparticles encapsulated in porous carbon derived from zeolitic imidazolate framework 67 for oxygen electroreduction in alkaline media. *J. Power Sources* 343, 458–466. doi: 10.1016/j.jpowsour.2017.01.081

Wang, L., Tang, Z., Yan, W., Yang, H., Wang, Q., and Chen, S. (2016). Porous carbon-supported gold nanoparticles for oxygen reduction reaction: effects of nanoparticle size. *ACS Appl. Mater. Interf.* 8, 20635–20641. doi: 10.1021/acsami.6b02223

Wang, S., Sun, W., Yang, D.-S., and Yang, F. (2019). Conversion of soybean waste to sub-micron porous-hollow carbon spheres for supercapacitor via a reagent and template-free route. *Mater. Today Energy* 13, 50–55. doi: 10.1016/j.mtener.2019.04.015

Wang, Y., Yin, X., Shen, H., Jiang, H., Yu, J., Zhang, Y., et al. (2018). Co_3O_4@g-C_3N_4 supported on N-doped graphene as effective electrocatalyst for oxygen reduction reaction. *Int. J. Hydrogen Energy* 43, 20687–20695. doi: 10.1016/j.ijhydene.2018.09.140

Wu, Z., Liu, R., Wang, J., Zhu, J., Xiao, W., Xuan, C., et al. (2016a). Nitrogen and sulfur co-doping of 3D hollow-structured carbon spheres as an efficient and stable metal free catalyst for the oxygen reduction reaction. *Nanoscale* 8, 19086–19092. doi: 10.1039/c6nr06817k

Wu, Z., Sun, L.-P., Yang, M., Huo, L.-H., Zhao, H., and Grenier, J.-C. (2016b). Facile synthesis and excellent electrochemical performance of reduced graphene oxide-Co_3O_4 yolk-shell nanocages as a catalyst for oxygen evolution reaction. *J. Mater. Chem. A* 4, 13534–13542. doi: 10.1039/c6ta04943e

Wu, Z., Wang, J., Song, M., Zhao, G., Zhu, Y., Fu, G., et al. (2018). Boosting oxygen reduction catalysis with N-doped carbon coated Co_9S_8 microtubes. *ACS Appl. Mater. Interf.* 10, 25415–25421. doi: 10.1021/acsami.8b07207

Xia, X., Shen, S., Lu, X., and Xia, H. (2017). Multiscale nanomaterials for electrochemical energy storage and conversion. *Mater. Res. Bull.* 96, 297–300. doi: 10.1016/j.materresbull.2017.09.045

Xiao, J., Kuang, Q., Yang, S., Xiao, F., Wang, S., and Guo, L. (2013). Surface structure dependent electrocatalytic activity of Co_3O_4 anchored on graphene sheets toward oxygen reduction reaction. *Sci. Rep*. 3:2300. doi: 10.1038/srep02300

Xie, S., Huang, S., Wei, W., Yang, X., Liu, Y., Lu, X., et al. (2015). Chitosan waste-derived Co and N co-doped carbon electrocatalyst for efficient oxygen reduction reaction. *ChemElectroChem* 2, 1806–1812. doi: 10.1002/celc.201500199

Xie, X., Li, Y., Liu, Z.-Q., Haruta, M., and Shen, W. (2009). Low-temperature oxidation of CO catalysed by Co_3O_4 nanorods. *Nature* 458, 746–749. doi: 10.1038/nature07877

Yu, M., Wang, Z., Hou, C., Wang, Z., Liang, C., Zhao, C., et al. (2017). Nitrogen-doped Co_3O_4 mesoporous nanowire arrays as an additive-free air-cathode for flexible solid-state zinc-air batteries. *Adv. Mater.* 29:1602868. doi: 10.1002/adma.201602868

Yu, P., Zeng, Y., Zhang, H., Yu, M., Tong, Y., and Lu, X. (2019). Flexible Zn-ion batteries: recent progresses and challenges. *Small* 15:1804760. doi: 10.1002/smll.201804760

Zhong, C., Deng, Y., Hu, W., Qiao, J., Zhang, L., and Zhang, J. (2015). A review of electrolyte materials and compositions for electrochemical supercapacitors. *Chem. Soc. Rev.* 44, 7484–7539. doi: 10.1039/c5cs00303b

Zhu, L., Zheng, D., Wang, Z., Zheng, X., Fang, P., Zhu, J., et al. (2018). A confinement strategy for stabilizing ZIF-derived bifunctional catalysts as a benchmark cathode of flexible all-solid-state zinc-air batteries. *Adv. Mater.* 30:1805268. doi: 10.1002/adma.201805268

Conflict of Interest: The authors declare that the research was conducted in the absence of any commercial or financial relationships that could be construed as a potential conflict of interest.